Journal of Glaciology

Article

Cite this article: Garg PK, Garg S, Yousuf B, Shukla A, Kumar V, Mehta M (2022). Stagnation of the Pensilungpa glacier, western Himalaya, India: causes and implications. *Journal of Glaciology* **68**(268), 221–235. https://doi.org/10.1017/jog.2021.84

Received: 18 August 2020
Revised: 15 June 2021
Accepted: 16 June 2021
First published online: 13 July 2021

Keywords:
Glacier stagnation; ice cliffs; multi-parametric assessment; Pensilungpa glacier; western Himalaya

Author for correspondence:
Purushottam Kumar Garg,
E-mail: garg.glacio@gmail.com,
Aparna Shukla,
E-mail: aparna.shukla22@gmail.com

cambridge.org/jog

Stagnation of the Pensilungpa glacier, western Himalaya, India: causes and implications

Purushottam Kumar Garg[1,2], Siddhi Garg[2], Bisma Yousuf[2], Aparna Shukla[2,3], Vinit Kumar[2] and Manish Mehta[2]

[1]Indian Institute of Technology Indore, Khandwa Road, Simrol, Indore 453552, Madhya Pradesh, India; [2]Wadia Institute of Himalayan Geology, 33 GMS Road, Dehradun 248001, Uttarakhand, India and [3]Ministry of Earth Sciences, Prithvi Bhavan, Lodhi Road, New Delhi 110003, India

Abstract

This study investigates stagnation conditions of the Pensilungpa glacier, western Himalaya. Multiple glacier parameters (length, area, debris extent and thickness, snowline altitude (SLA), velocity, downwasting and ice cliffs) were studied using field measurements (2016–18), high-resolution imagery from GoogleEarth (2013–17) and spaceborne Landsat, ASTER and SRTM data (1993–2017) to comprehend the glacier's current state. Results show a moderate decrease in length (6.62 ± 2.11 m a^{-1}) and area ($0.11 \pm 0.03\%$ a^{-1}), a marked increase in SLA (~6 m a^{-1}) and debris cover ($2.86 \pm 0.29\%$ a^{-1}) and a slowdown of ~50% during 1993–2016. Notable thinning of -0.88 ± 0.04 m a^{-1} was observed between 2000 and 2017 showing a similar trend as field measurements during 2016–17 (−0.88 m) and 2017–18 (−1.54 m). Further, results reveal a stagnation of the lower ablation zone (LAZ). Less mass supply and heterogeneous debris growth ($6.67 \pm 0.41\%$ a^{-1}) over the previous decade resulted in slowdown, margin insulation and slope-inversion, leading to stagnation. Stagnation of LAZ caused bulging in the dynamic upper ablation zone and favored the development of supraglacial ponds and ice cliffs. Ice cliffs have grown significantly (48% in number; 41% in area during 2013–17) and their back-wasting now dominates the ablation process.

1. Introduction

Debris cover is a pertinent feature of Himalayan glaciers. About 10% of the total Himalayan glacierized area and ~40% of ablation areas are debris-covered with varying debris thickness ranging from a few centimeters to tens of centimeters (Bolch and others, 2012; Sharma and others, 2016; Miles and others, 2017). There have been ample reports of continuous debris increase on the Himalayan glaciers (Bhambri and others, 2011; Ali and others, 2017; Patel and others, 2018; Garg and others, 2019). Debris cover generally appears below the equilibrium line and can play an active role in modifying the ablation processes and overall morphology of the ablation tongues. Debris thickness pattern on debris-covered glacier tends to transition from convex- to concave-up-down glacier (Anderson and Anderson, 2018) which may lead to differential downwasting and may cause slope inversion (Benn and others, 2012). The changing ablation patterns and morphology can influence the glaciers' surface ice velocity (SIV). Previous studies clearly report progressive slow-down and stagnation of debris-covered glaciers in the Himalaya (Quincey and others, 2009; Scherler and others, 2011; Bhattacharya and others, 2016; Bhushan and others, 2017; Garg and others, 2017). Stagnation has been defined as a very slow movement of the glacier. Obviously, there will be some movement in the ice for it to be considered a part of the glacier instead of 'dead ice'. However, previous studies have adopted different thresholds of velocity to distinguish the stagnant portion of the glaciers. Scherler and others (2011) termed a glacier portion stagnant if the velocity is <2.5 m a^{-1}. Quincey and others (2009) did not specify a threshold, but designated lower debris-covered glacier tongues to be stagnant if these are moving very slowly (possibly <5 m a^{-1} as Fig. 3 in Quincey and other (2009) depicts). Shukla and Garg (2019) defined SIV <10 m a^{-1} as a 'very slow movement'. In the present study, we term a glacier part as stagnation if the SIV is <5 m a^{-1}. Glacier stagnation can lead to a stable glacier terminus but such glaciers are susceptible to evolve new mass loss mechanism such as formation and development of ice cliffs. Ice cliffs, in turn, can account for ~7–40% of total wastage of a debris-covered portion (Immerzeel and others, 2014; Thompson and others, 2016; Steiner and others, 2019). Thus, it is important to identify the stagnant conditions of glaciers, the various processes leading to glacier stagnation and the consequences of stagnation.

Glacier response to climate changes is manifested through changes in glacier length, area, debris cover, SIV, surface elevation, snowline altitude (SLA) and formation/development of associated glacial lakes. Given the harsh environmental conditions of glaciated regions, the study of glacier parameters on the field is challenging and costly. This makes remote sensing perhaps the only viable alternative to study the glacial characteristics periodically (Paul and others, 2013; Shukla and Qadir, 2016). However, serious concern here is that most of the efforts in the Himalaya pertaining to remote sensing have been made toward assessing the dimensional changes (i.e. length and area) only (Vincent and others, 2013; Garg and others, 2019). Dimensional variations are the simplest way of monitoring mountain glacier changes

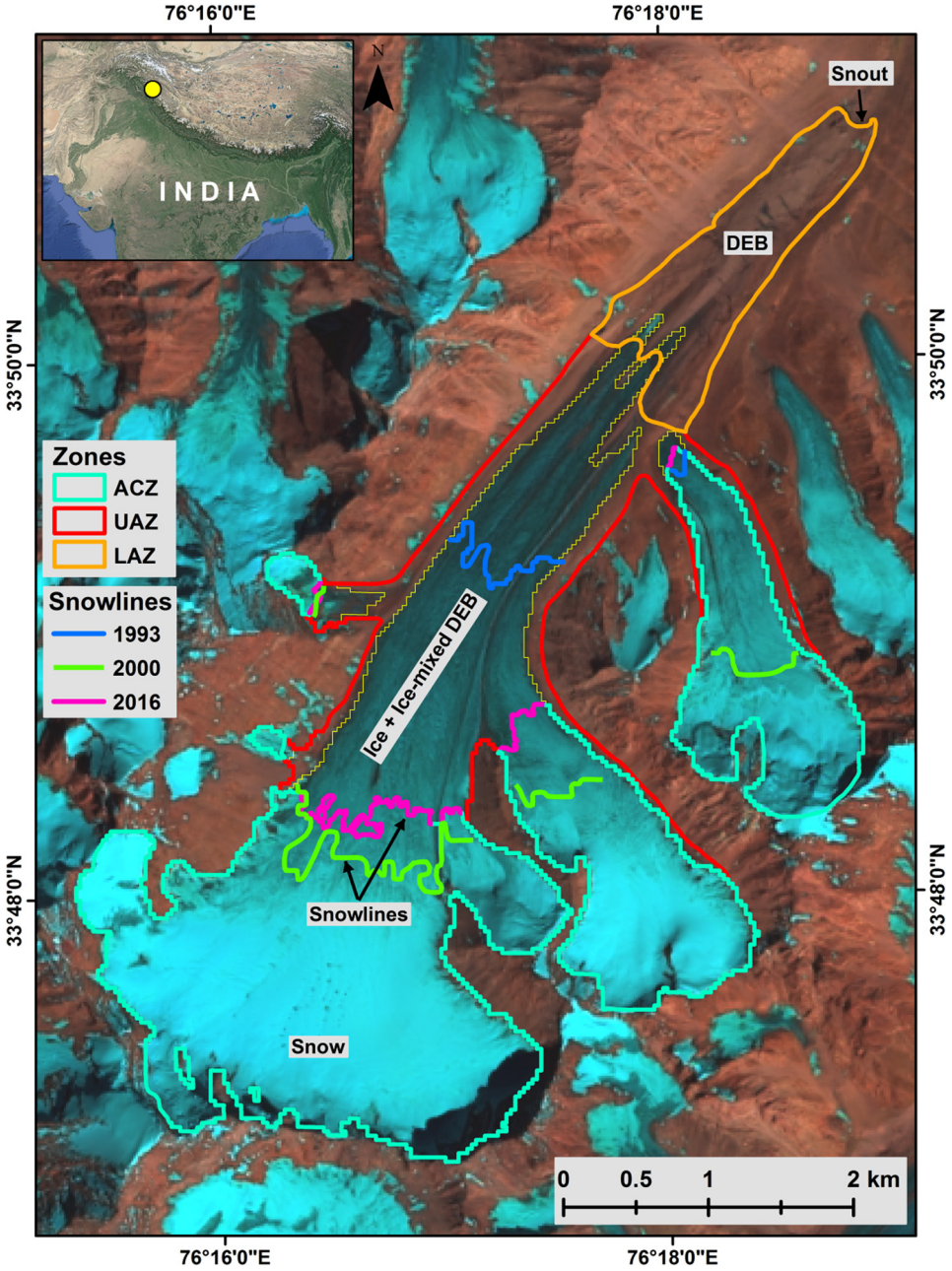

Fig. 1. Location of the study area. The glacier and debris cover (DEB) outlines overlain on map are of the year 2016. The background is a Landsat OLI image of 8 October 2016. Lower ablation zone (LAZ), upper ablation zone (UAZ) and accumulation zone (UAZ) and snowlines are also shown on the map.

and have been used to infer climatic signals on both regional and global scales (Hoelzle and others, 2003; Leclercq and Oerlemans, 2012). However, it is necessary to note that these changes provide indirect, delayed and filtered responses of glaciers and are not a comprehensive assessment of the total glacier condition or health (Armstrong, 2010; Zemp and others, 2015). Moreover, several recent studies have indicated that glaciers with apparently stable fronts may also lose significant mass through downwasting (Bolch and others, 2011; Kargel and others, 2011; Immerzeel and others, 2014). Therefore, a multiparametric study is required in order to understand the comprehensive glacier response to climate change.

In the present study, the Pensilungpa glacier in the Suru river sub-basin has been selected for a detailed investigation. The study area falls in the monsoon-arid zone making it important for climate change-related studies (Pandey and others, 2011; Shukla and Qadir, 2016). Considering the above-described aspects, the main goals of this paper are to (a) present a comprehensive picture of status and behavior of the Pensilungpa glacier by monitoring multiple glacier parameters namely length, area, SLA, SIV and surface elevation changes (SEC), (b) understand the influence of changing glacier parameters on the stagnation/ablation process and (c) evaluate the stagnant conditions of the glacier and its implications.

2. Study area and datasets

The Pensilungpa glacier (terminus coordinates: 33.845°N, 76.375°E) is a medium-sized (length: 8.51 km; area: 14.67 ± 0.29 km^2 in 2016) valley-type glacier located in the Kargil district of Jammu and Kashmir (Fig. 1). It is situated near the Pensi-La pass, which is often referred to as the 'Gateway to Zanskar' (Kamp and others, 2011). The glacier surface is highly undulating and crevassed (Fig. 2). As per recent estimates (2016) of the present study, ~17.35% of total area of this glacier is covered with debris comprising fine-grained sand to large boulders (Fig. 2). The

https://doi.org/10.1017/jog.2021.84 Published online by Cambridge University Press

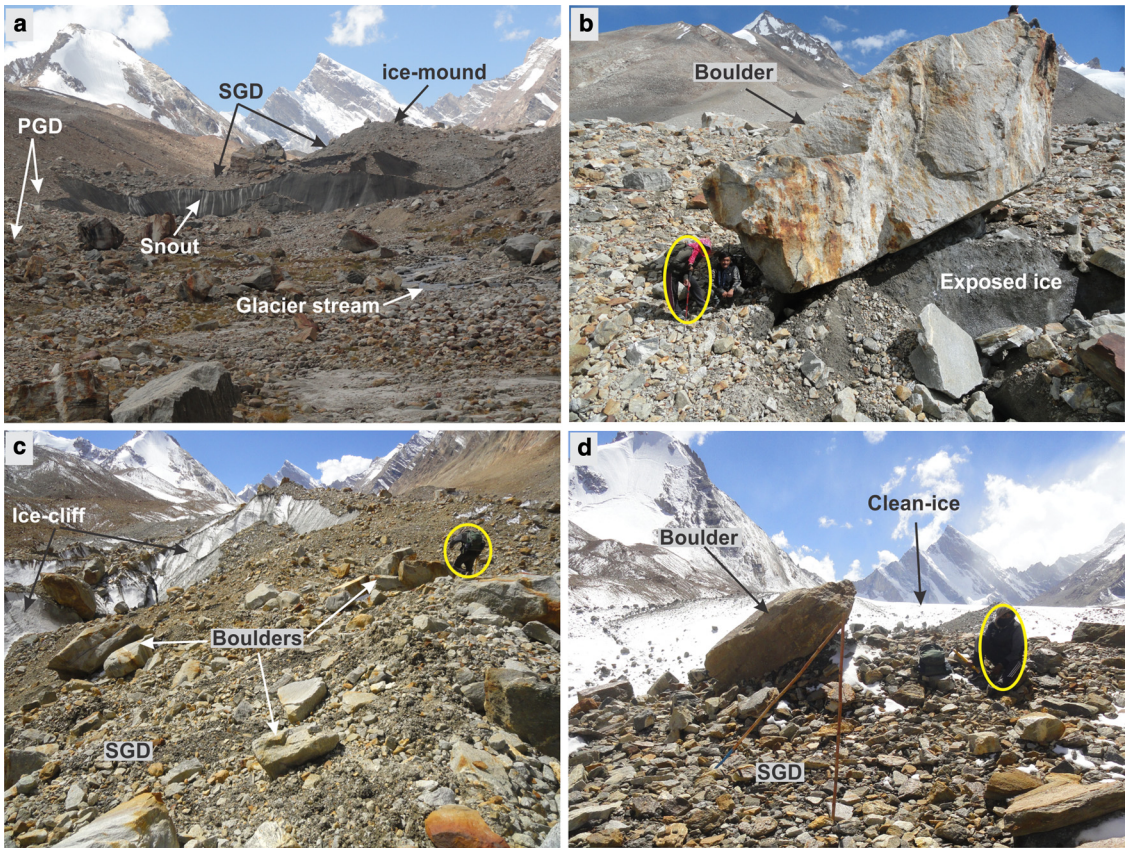

Fig. 2. Debris cover characteristics over the Pensilungpa glacier. Notice a large variation in the size of debris mantle ranging from a few millimeter to big boulders of several meters. Yellow ellipsoids marked on the photographs show human scale.

glacier flows north-east from an elevation of ~6000 m above sea level (a.s.l.) and terminates at 4668 m a.s.l. giving rise to the Suru River, which is an important tributary of the River Jhelum. The SLA of glacier is at 5160 m a.s.l. (2016) which divides glacier into accumulation zone (ACZ) and ablation zone (ABZ). The ABZ has been further divided into lower ablation zone (LAZ) and upper ablation zone (UAZ) considering the distinctive dynamics and geomorphological features of these zones as deduced in an integrative manner from the field and remote-sensing data (Fig. 1). The LAZ is characterized by a debris mantle of heterogeneous thickness but following the thinning upwards trend and very low SIVs (<5 m a^{-1}). It has uneven and quite rugged topography probably owing to the unequal amount of surficial melting. Ice cliffs with varying aspects and trends, glacier tables, deep supraglacial channels and ephemeral meltwater accumulations/ponds are common occurrences in LAZ. While UAZ has relatively much smoother surface with very sparse debris cover, higher SIVs and a narrow and shallow network of supraglacial channels. The drop down in SIV at ~2 km from the snout (discussed in Section 4.2) is a clear indication of the transition from LAZ to UAZ; however, according to the field observations, the boundary between these two zones is fuzzy and not sharp. This is because surface feature characteristics of the LAZ continue for ~150–200 m beyond the maximum debris cover extent. Thus, the boundary between LAZ and UAZ roughly follows the debris cover extent and has an average elevation of ~4905 m a.s.l. (Fig. 1).

The prime reason for selection of this particular glacier for our study includes its accessibility (~150 km by road from Kargil town), medium size, well-defined ACZ and ABZ, and locality in the climatically crucial rain-shadow (semi-desert) zone (Archer and Fowler, 2004). The region alternatively receives snowfall during winter and rainfall during summer from westerlies and Indian summer monsoon (ISM), respectively. The average annual precipitation, recorded at the Leh meteorological station of this region, amounts only to ~250 mm (Shukla and Qadir, 2016). Due to alternate influence of westerlies and ISM, the region experiences an annual temperature range from a winter minimum of 1.3 to −7.8°C to a summer maximum of 8.0–18.2°C. Shukla and others (2020) reported that the mean annual temperature in study region increased by 0.8°C over the period 1901–2017. The mean annual minimum temperature registered higher increase (1.3°C) than the mean annual maximum temperature (0.3°C) along with a simultaneous increase in the precipitation (~20%) during this period. Moreover, a conspicuous temperature rise after 1996 occurred in the region (Shukla and others, 2020).

Gridded temperature and precipitation data from the Climate Research Unit (CRU) Time Series 4.01 (TS 4.01) having spatial extent of 0.5° × 0.5° latitudinal and longitudinal grids, covering the study region, have also been analyzed here for 1901–2016 period. The climate data show an annual average precipitation and temperature of 441 mm and 0.6°C, respectively, over the 115 years. Precipitation is observed in almost all the months with maxima in the months of July and August, followed by January and February. Also, July is the warmest while January is the coldest month in the region (Fig. 3). It is notable that the long-term temperature for November–April months remains well below 0°C (Fig. 3). Therefore, it can be inferred that these months likely receive solid precipitation. Conversely, temperature for the May–October months remains above 0°C (Fig. 3) indicating a likelihood of receiving liquid precipitation.

The study aims at evaluating glacier parameters for 1990, 2000 and 2015 time periods by utilizing remote-sensing data from various satellites and sensors. However, in case of unavailability of

https://doi.org/10.1017/jog.2021.84 Published online by Cambridge University Press

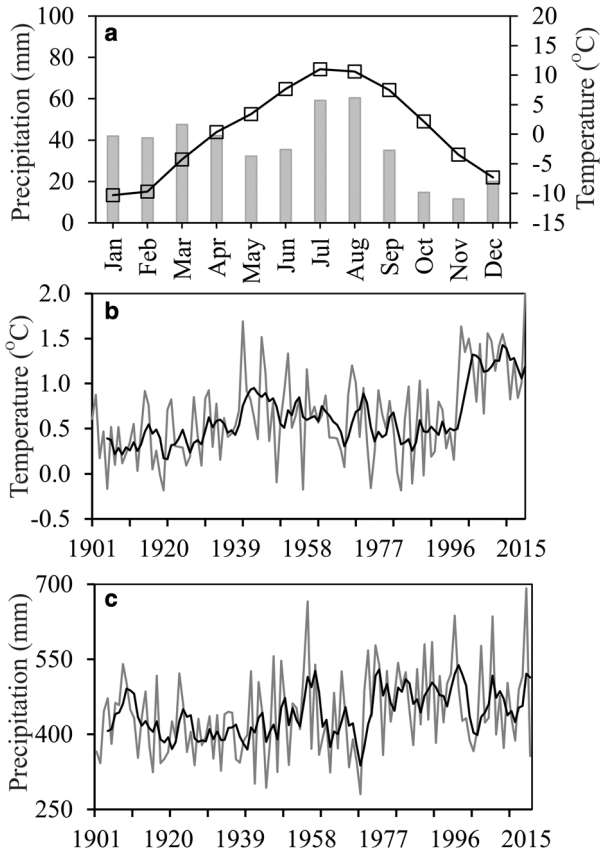

Fig. 3. Temperature and precipitation data for the study region acquired from CRU TS 4.01 dataset for the period of 1901–2016. Notice a continuous increase in temperature and almost no change in the precipitation, particularly in the recent decades. The step change in temperature after 1996 is particularly noticeable and corresponds well with previous studies (Bhutiyani and others, 2010; Harris and others, 2014; Shukla and others, 2020). Solid black lines show 5-year moving average plots.

suitable (i.e. snow and cloud free) images, we had to use the next suitable images having 3–4 years gap from the target years. For estimation of glacier area, length, debris cover, snowlines and SIV, Landsat data from thematic mapper (TM; 1990 ± 4 years), Enhanced Thematic Mapper Plus (ETM +; 2000 ± 4 years) and Operational Land Imager (OLI; 2015 ± 4 years) have been utilized. All the Landsat images were acquired from the Earth Explorer website (https://earthexplorer.usgs.gov/). The SEC was quantified by subtracting Shuttle Radar Topographic Mission (SRTM) Digital Elevation Model (DEM) version-3 (v3) of 2000 from Advanced Spaceborne Thermal Emission and Reflection Radiometer (ASTER) DEM of 2017. The ASTER DEM was downloaded from the Earth Data website (https://search.earthdata.nasa.gov/). The SRTM DEM has been used here as the reference DEM and acquired from https://earthexplorer.usgs.gov/ which possesses a vertical accuracy of ±10 m (Rodriguez and others, 2006). The AST14 DMO product was used here as a secondary DEM and was procured from the https://search.earthdata.nasa.gov/. Table 1 lists the complete details of remote-sensing data used in this study. Further, considering the dynamic nature of SLA, we have carried out its time series mapping between 1993 and 2016 using diverse remote-sensing data (Supplementary Table S1).

Field observations are required to closely understand the glacier characteristics and to address inherent uncertainties involved in mapping the glacier parameters from remotely sensed data. Field work campaigns to the Pensilungpa glacier were undertaken during the months of August–September in 2016, 2017 and 2018. Several glacier features were observed and photographed to understand the glaciers' current state (Figs 2, 4). Also, stakes were installed on the ABZ of the glacier in 2016 and 2017 and tracked using a Leica Geosystem Differential Global Positioning System (DGPS), which provides horizontal and vertical accuracies of ±10 and ±5 cm, respectively, in a mountainous terrain. A total number of ten ablation stakes were installed in the LAZ (4668–4905 m a.s.l.) of the glacier in 2016 which were measured in 2017 to calculate the annual point melting. In 2017, nine stakes could be measured as one stake was lost. Further, in addition to nine previously installed stakes, eight more stakes were installed in 2017 to cover the entire debris-covered portion of the glacier including some parts of UAZ. However, in 2018, only 11 stakes could be recovered.

3. Methodology

3.1. Glacier parameter extraction

Glacier boundaries (i.e. glacier area) were mapped in a two-step process. In the first step, we created band ratios using Red and Shortwave Infrared Bands (Red/SWIR) and applied a scene-specific threshold (ranging from 1.6 for OLI to 1.9 for TM) to automatically identify the clean-ice parts. The raster files thus generated were smoothened using a median filter (3 × 3) and converted to vector polygons followed by manual corrections of misclassified polygons (Bhambri and others, 2011; Chand and Sharma, 2015). In the second step, debris-covered parts were digitized manually using various key features such as rough texture of debris, flow patterns, impression of ice cliffs and melt-water stream (Pandey and Venkataraman, 2013; Paul and others, 2013; Chand and Sharma, 2015). The debris-covered area was estimated by differencing the manually (debris-covered parts) and semi-automatically (debris-free portion) estimated glacier extents. The uppermost boundary of the glacier was kept fixed, and the temporal glacier changes were estimated for the other parts as no visible change could be identified in the upper accumulation region because of seasonal snow cover (Chand and Sharma, 2015). Temporal glacier boundaries were compared to calculate the area changes. Glacier length was estimated along the manually digitized central flowline starting from bergschrund to the snout while length change (i.e. retreat) was estimated using parallel strips having 50 m offset (Garg and others, 2019; Kaushik and others, 2019). The snowlines were also identified and digitized manually on all the images, while their elevation was extracted from SRTM DEM-v3 using a one pixel buffer (Rabatel and others, 2013; Shukla and Qadir, 2016). The SLA fluctuation was estimated by (a) direct comparison between temporal SLA for the years 1993, 2000 and 2015 and (b) taking the average of SLA variation between consecutive mapping years.

The SIVs were estimated by correlating temporal Landsat images using Co-registration of Optically Sensed Images and Correlation (COSI-Corr) (Leprince and others, 2007; Tiwari and others, 2014). Table 2 shows the correlated velocity pairs. After investigating various combinations, window sizes of 64 × 16 pixels for TM (NIR band) and 64 × 32 pixels for ETM+ and OLI (Panchromatic band) were found to be optimum in this study. The north-south (NS) and east-west (EW) displacements (resulting from correlations) were resampled to 60 m ground resolution. During post-processing, series of corrections were applied on the displacement images. Firstly, low-signal-to-noise ratio (SNR < 0.90) values were filtered out to remove poorly correlated pixels. Pixels with displacement >200 m were also masked out to exclude outliers. Then, the wave artefacts prevalent in the along-track direction, introduced from residual attitude effect of sensors, were also modeled using pixels from stable ground. After that, a directional filter was applied on the velocity products. Finally, the

https://doi.org/10.1017/jog.2021.84 Published online by Cambridge University Press

Table 1. List of satellite data used in this study

Satellite/sensor	Scene ID	Date of acquisition	Parameter estimated
Landsat/TM	LT51480371993236ISP00	24 August 1993	Length, area, DC, SL, SIV
Landsat/TM	LT51480371994207ISP00	26 July 1994	SIV
Landsat/ETM +	LE71480371999229AGS00	17 August 1999	SIV
SRTM		February 2000	SEC, SLA
Landsat/ETM +	LE71480372000248SGS00	04 September 2000	Length, area, DC, SL, SIV
Landsat/OLI	LC81480372016252LGN00	08 September 2016	Length, area, DC, SL, SIV
Landsat/OLI	LC81480372017302LGN00	29 October 2017	SIV
Terra/ASTER	AST14DMO_00309192017054750_ 20171127050600_30905	19 September 2017	SEC

DC, debris cover; SL, snowline; SLA, snowline altitude; SIV, surface ice velocity; SEC, surface elevation change.

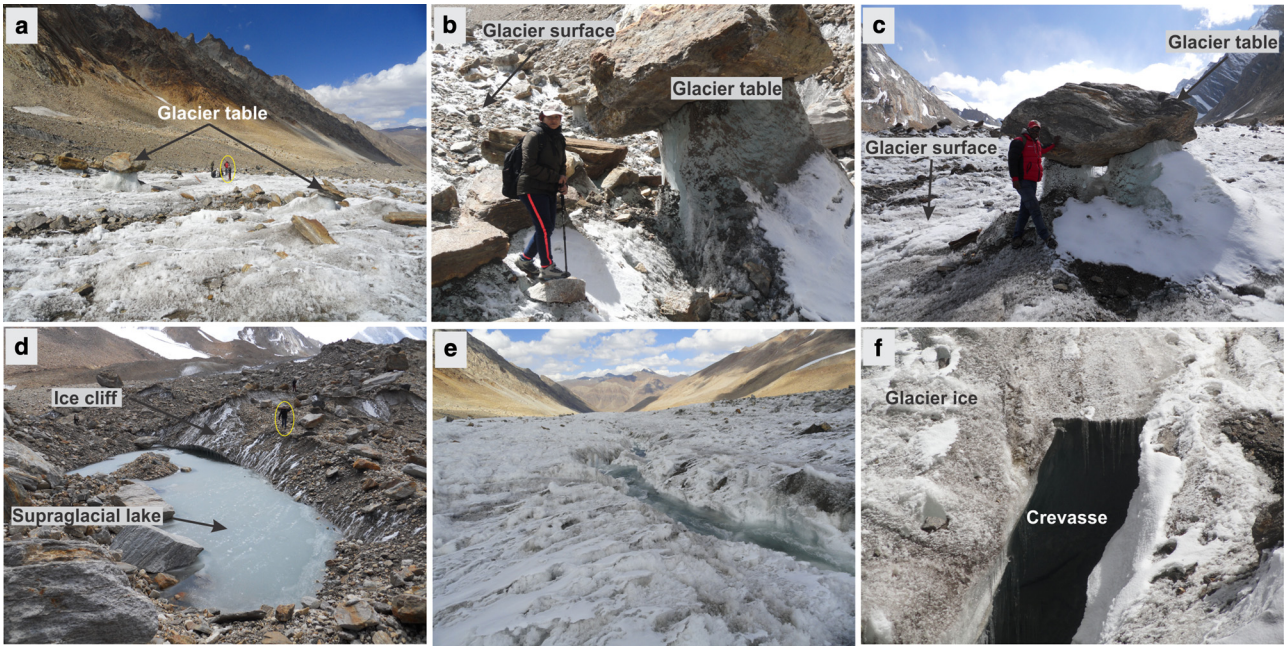

Fig. 4. Various glacial features such as (a–c) glacier tables, (d) glacial pond and associated ice cliffs, (e) supraglacial channel and (f) deep crevasse, observed during the field visit on the Pensilungpa glacier during the months of August–September in 2016 and 2017. The human scale is marked on the photographs (panels a and d) as yellow ellipsoids. Glacier tables with significant height (up to 2–2.5 m) clearly indicate differential melting and pronounced downwasting on the glacier.

Table 2. List of image-pairs used in this study to estimate the surface ice velocity (SIV) of the Pensilungpa glacier

Period	Image-pair Pre event	Post event	N_{stable}	M_{stable}	$STDEV_{stable}$	U_{SIV} (U_{SIV} = M_{stable} + $STDEV_{stable}$)
1990	24 August 1993	26 July 1994	10 883	2.63	1.34	3.97
2000	17 August 1999	04 September 2000	10 883	1.58	1.18	2.76
2015	08 September 2016	29 October 2017	10 883	4.96	1.96	3.87

N_{stable}, number of pixels from stable terrain; M_{stable}, mean SIV over selected stable pixels; $STDEV_{stable}$, std dev. of SIV over stable pixels.
The uncertainties (U_{SIV}) associated with each pair are also given in the table.

annual SIVs were computed as per the following:

$$SIV = \left(\frac{\sqrt{NS^2 + EW^2}}{n}\right) \times 365, \quad (1)$$

where n = temporal separation (in days) between the correlated images, NS = north-south displacement and EW = east-west displacement. The velocity of the Pensilungpa glacier was calculated along the central flowline and resampled at every 300 m from the snout. Apart from this, we have also estimated SIV from field stake measurements for 2016/17 to validate our remotely-derived SIV for the corresponding year. First, we computed surface ice displacement (D_{field}) using stake coordinates recorded during 2016 (T_1) and 2017 (T_2) as per Eqn (2) and subsequently converted into velocity (V_{field}) using Eqn (3).

$$D_{field} = \sqrt{(X - X_2)^2 - (Y_1 - Y_2)^2}, \quad (2)$$

$$V_{field} = \frac{D_{field} \times 365}{(T_1 - T_2)}, \quad (3)$$

where X_1, Y_1 and X_2, Y_2 represent the coordinates of the stakes for T_1 (2016) and T_2 (2017), respectively.

The SEC of the Pensilungpa glacier was determined by comparing the AST14 DMO of 2017 and SRTM DEM of 2000. The

https://doi.org/10.1017/jog.2021.84 Published online by Cambridge University Press

Table 3. Statistics of the surface elevation differences on the stable terrain for the raw and corrected difference images

Elevation difference (stable terrain)		Raw	Corr. 1	Corr. 2	Corr. 3	Corr. 4	Corr. 5	Total improvement in SD (%)
2017 ASTER−2000 SRTM	X	−13.33	−3.33					
	Y	20.00	−3.33					
	Mean (m)	−7.35	0.03	−0.07	−0.33	−0.10	−0.14	
	SD (m)	33.24	31.10	21.13	21.11	21.16	20.80	
	Improvement in SD		6.43	32.05	0.11	−0.23	1.67	37.41

Corrections (Corr.) 1–5 respectively denote the co-registration, spatial trend, elevation, slope, aspect and curvature-related error corrections. The improvement in std dev. (SD) denotes the improvement of each correction compared to the previous step.

ASTER DEM was first smoothened using a median filter (3 × 3). Then the peaks and sinks were identified by creating a hillshade image and removed using spline method (Racoviteanu and others, 2009; Paul and others, 2013). Both the DEMs were co-registered by minimizing the std dev. of the elevation difference over the least error-prone ice-free stable and low sloping areas to achieve horizontal congruence (Berthier and others, 2016). For this, several masks including glacier mask (GLIMS glacier boundaries for the year 2000; GLIMS, 2015), slope mask (<4° and >45°), cloud mask (manually digitized) and outlier mask (±100 m) were applied on the elevation difference image. After the planimetric adjustment, along/cross track corrections were incorporated by rotating the coordinate system of the ASTER DEM using azimuth of ASTER ground track and estimating elevation difference over stable areas (Nuth and Kääb, 2011; Kumar and others, 2017). Following this, elevation, slope and curvature-dependent vertical biases were removed from the SEC using all reliable measurements over stable areas (Gardelle and others, 2013). During vertical adjustment, the range of outlier mask was narrowed down to ±50 m to have more reliable pixels form stable ground. Table 3 shows the improvement in the std dev. after each correction. The SRTM was created using C-band which potentially underestimates the glaciated terrain due to its varying penetration depth into different glacier classes (i.e. snow, firn, debris), causing one of the most important uncertainty sources (Gardelle and others, 2013; Vijay and Braun, 2016; Zhou and others, 2018). Therefore, to account this error, here we have employed penetration depth correction of 2.3 ± 0.6 m for snow, 1.7 ± 0.6 m for clean-ice and 0.4 ± 0.8 m for debris-covered glacier parts, which is equal to an average penetration depth of ±1.46 m (Kääb and others, 2012; Gardelle and others, 2013; Zhou and others, 2018). Further, the SRTM was acquired in the month of February and the ASTER DEM used here was acquired in the month of September. The potential mass accumulation during these 5 months requires seasonality correction. In the present study, we applied a correction factor of 0.15 m w.e. per winter month as discussed in Gardelle and others (2013) and Zhou and others (2018). Figure 5 shows the elevation difference before and after the corrections. Finally, the SECs for the concerned glacier were calculated along the central flowline averaged for every 200 m distance from the snout.

3.2. Uncertainty estimation

Quantifying uncertainties associated with remotely derived glacier parameters bears prime importance in substantiating the results (Paul and others, 2013; Shukla and Qadir, 2016; Kaushik and others, 2019). Here, the uncertainties in glacier area and debris cover mapping were estimated using buffer method (Chand and Sharma, 2015; Garg and others, 2019). The buffer size, equivalent to the coregistration error of 6 m (Storey and Chaoate, 2004; Heid and Kääb, 2012; Bhattacharya and others, 2016), was set. This yielded the uncertainties in glacier area and debris cover estimation as 1.96, 2.02 and 2.10% for 1990 TM, 2000 ETM+ and 2016 OLI.

The uncertainties in temporal area and debris cover changes were quantified as per Hall and others (2003) which comes to ±0.0029 km^2 for both the time periods (i.e. 1993–2000 and 2000–16). The uncertainties in snout retreat were also calculated according to Hall and others (2003) which come as ±2.14 m a^{-1} for 1993–2016, ±6.79 m a^{-1} for 1993–2000 and ±3.24 m a^{-1} for 2000–2016 period. The SLA uncertainties can be realized as ±10 m in the vertical (equal to the vertical accuracy of DEM) and ±15 m in the horizontal direction (equal to the buffer size used).

We estimated the uncertainties associated with SIVs as per Scherler and Strecker (2012) and Garg and others (2017) wherein the displacement and std dev. over stable terrain were added and divided by temporal separation of the correlated image-pairs (Table 2). The resultant values varied from ±2.76 m a^{-1} in 2000 to ±3.97 m a^{-1} in 1990. Relatively higher uncertainty in 1990 may be attributed to the partial snow and cloud cover in that image. The uncertainty in SEC (U_{SEC}) has been estimated according to Bolch and others (2011) and Bhushan and others (2018) using mean (M; −0.14 m) and std dev. (SD; 20.80 m) of elevation difference over stable terrain (number of pixels (n) = 1840471). We first computed standard error (SE) as $SE = SD/\sqrt{n}$ to be 0.02 m and then relative error in elevation difference (E_{SEC}) as $E_{SEC} = \sqrt{SE^2 + M^2}$ to be 0.14 m. Finally, U_{SEC} was estimated as $U_{SEC} = \sqrt{(E_{SEC})^2 + (E_p)^2 + (E_s)^2}$ considering the errors in penetration (E_p; 0.6 m) and seasonality correction (E_s; 0.15 m). Accordingly, the U_{SEC} was computed to be 0.63 m (±0.04 m a^{-1}).

4. Results

4.1. Glacier length, area debris cover and SLA changes

Results reveal that the total length of the Pensilungpa glacier was 8.66 ± 0.03 km in 1993. Over the monitoring period (1993–2016), the glacier retreated at a rate of 6.62 ± 2.11 m a^{-1} leading to a total length reduction of 152.20 ± 48.43 m. The retreat rate increased from 5.16 ± 6.92 a^{-1} during 1993–2000 to 7.25 ± 3.03 m a^{-1} during 2000–16. The glacier area was 15.06 ± 0.28 km^2 in 1993 which reduced to 14.89 ± 0.28 km^2 in 2000 and further to 14.67 ± 0.29 km^2 in 2016. This shows that, in aggregate, the glacier lost 2.56 ± 0.75% (0.11 ± 0.03% a^{-1}) of its total area during the study period.

In 1993, 10.47% (1.58 ± 0.03 km^2) of the total glacier area was covered by debris. Accompanying the glacier recession, the supraglacial debris also increased to 15.36% (2.29 ± 0.04 km^2) in 2000 and to 17.35% (2.55 ± 0.05 km^2) in 2016, revealing an average annual debris growth of 2.86 ± 0.29% a^{-1}. On a decadal timescale, the debris expansion was higher (6.67 ± 0.41% a^{-1}) during 1993–2000, and dropped to 0.81 ± 1.12% a^{-1} during 2000–16.

The average SLA of the glacier was 5197 ± *73.57* m a.s.l. (std dev. italicized) for the period 1993–2016. As expected, there is significant annual variability in SLA over the study period

https://doi.org/10.1017/jog.2021.84 Published online by Cambridge University Press

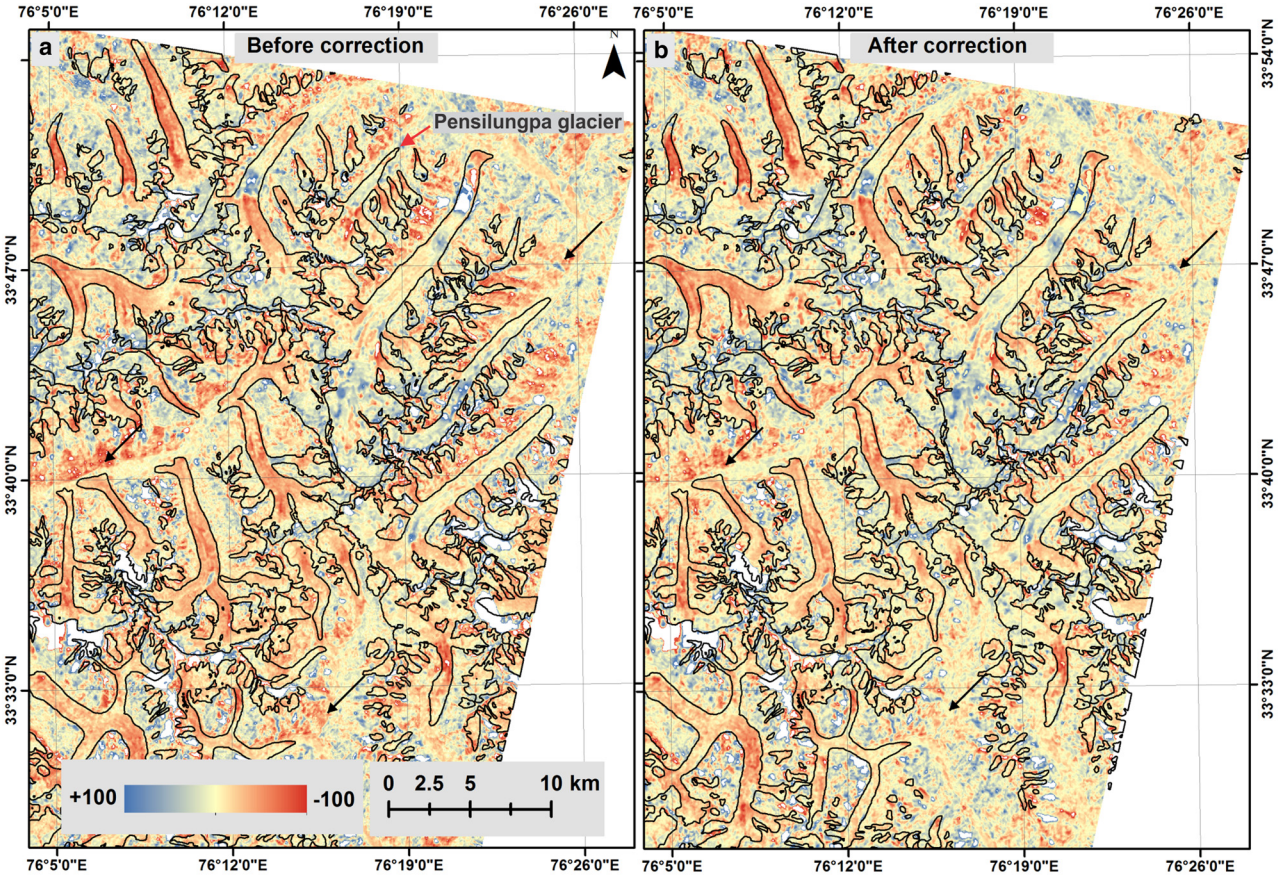

Fig. 5. Map showing (a) raw and (b) corrected elevation difference images deduced by differencing 2000 SRTM DEM from 2017 ASTER DEM. The various corrections include 3-D coregistration, along/across track, elevation, slope and terrain curvature-related error corrections. A good congruence between the temporal DEMs can be seen on stable terrain. Black arrows on the map show sites of improvement. The black polygons show the glacier masks from GLIMS for the year 2000 (GLIMS, 2015; https://www.glims.org/).

(Supplementary Fig. S1). Maxima and minima in SLA were attained during 2008 (5310 ± *76* m a.s.l.) and 1993 (5023 ± *20* m a.s.l.), respectively. Overall, the SLA has increased by 137 m in elevation between 1993 and 2016. It can be inferred from the time series SLA that rapid average upshift (between two consecutive years) of 36 m occurred between 1993 and 2000 while SLA descended on an average by 4 m during 2000–2016. Field measurements for the year 2016/17 and 2017/18 suggest the equilibrium line altitude (ELA) to be at 5215 and 5223 m a.s.l., respectively. Field-ELA for 2016/17, though differing from remotely-derived SLA by 56 m, confirms a clear upshift as compared to SLAs of 1993 and 2000. The observed shift between the field and remotely sensed ELAs may be attributed to (a) the difference in the nature of the two, i.e. in field, the elevation representing actual transition between accumulation and ablation is estimated, while using satellite images, the end of season snow line is mapped; (b) the field ELA estimation seldom takes the tributary glaciers into consideration while remotely derived ELA considers the entire boundary between ACZ and ABZ across tributaries.

4.2. SIV and SEC

The SIV of Pensilungpa glacier could only be estimated upto ~5 km distance from snout (Fig. 6a), as the presence of snow in the ACZ resulted in poor correlations. Results reveal that initially (in 1993/94) the glacier was moving with an average speed of 14.23 ± 3.97 m a^{-1}, which reduced to 11.56 ± 2.76 m a^{-1} in 1999/00 and further to 7.86 ± 3.87 m a^{-1} in 2016/17. These values are the mean of all reliable measurements obtained for the respective time periods. However, for inter-comparison of temporal SIVs, we have considered only those glacier parts for which good correlations were obtained in all the three time periods. This shows the average SIV to be 13.94 ± 3.97, 9.33 ± 2.76 and 7.63 ± 3.87 m a^{-1} in 1993/94, 1999/00 and 2016/17, respectively. Thus, the results confirm a total decrease in the glacier velocity by 48.28% (1.97% a^{-1}) between 1993/94 and 2016/17. Spatially, the maximum SIV has been observed in the UAZ (4905–5160 m a.s.l.) or middle part of the glacier while LAZ (4668–4905 m a.s.l.) remained stagnant in all the monitoring periods (Fig. 6a). Further, the SIV for 2016/17 has also been monitored in the field. In total, we could compute field-SIV for 9 stake points located on the LAZ. The average field-SIV is calculated to be 2.81 ± 1.22 m a^{-1}. The remotely-derived SIV for the same year and for the corresponding points is 3.85 ± 3.87 m a^{-1}. Thus, SIV estimates from both approaches reveal very slow movement of the LAZ and, hence, complement each other.

The glacier SEC has been evaluated between 2000 and 2017 which reveals a thinning of −0.88 ± 0.04 m a^{-1}. We interpret this thinning as predominantly downwasting (see Sections 5.2 and 5.3) and therefore use the term downwasting here as well. The maximum lowering is observed to be concentrated in the UAZ of the glacier (2–5 km upstream from snout) (Fig. 6b). The debris-covered lower portion of the glacier has shown comparatively less lowering. Nevertheless, significant lowering (average −15.75 ± 0.68 m) was noticeable near the snout region, particularly in ~120 m stretch from snout (Fig. 6b), which is likely because of the observed terminal retreat (116 m during 2001–

https://doi.org/10.1017/jog.2021.84 Published online by Cambridge University Press

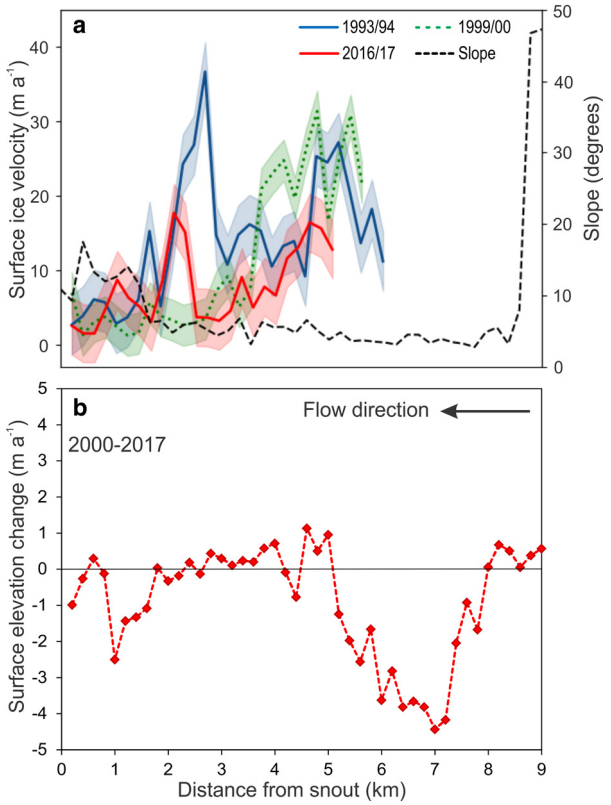

Fig. 6. (a) Surface ice velocity (SIV) of Pensilungpa glacier during 1993/94, 1999/00 and 2016/17 deduced by correlating temporal remote-sensing images, (b) surface elevation change on glacier obtained by subtracting 2000 SRTM digital elevation model (DEM) from 2017 ASTER DEM. Note an almost stagnant condition in the lower ablation zone (upto ~2 km) in panel (a). The stagnant position is also evident in the elevation difference map (panel b). The observed lowering between 1 and 2 km distance from snout may be attributed to the backwasting of ice cliffs.

2016) and ongoing processes of cave collapsing near the snout region.

Measurements taken in the field show a clear downwasting (evidenced from nine recovered stakes in 2017) ranging from −0.54 to −1.53 m (average: −0.88 m) during 2016–2017. However, these points mainly covered the lower debris-covered portion of the glacier where the debris thickness is much higher (Fig. 7). During 2017–2018, where the network of stakes was expanded to cover the upper thinly debris-covered portion of the glacier, an enhanced average downwasting of −1.54 m was observed with an incredible downwasting of ~>3 m on stake points where the debris thickness was <5 cm (Fig. 7). The average geodetic lowering on corresponding field points was estimated to be -0.63 ± 0.04 and -0.71 ± 0.04 m a^{-1}, respectively, which is also in conformity with field-derived downwasting trend and magnitude.

5. Discussion

5.1. Comparison with previous studies

Several past studies have attempted to assess the dimensional changes of the Pensilungpa glacier as well as other glaciers in its vicinity. Table 4 compares the results of length and area change of present study to that of the previous ones. Our length estimates differ considerably from Kamp and others (2011) and Pandey and others (2011). These discrepancies have also been previously recognized by Shukla and Qadir (2016). The study by Kamp and others (2011) reported that the Pensilungpa glacier retreated by almost ~1 km (946 m in absolute term) between 1992 and 2006 while Pandey and others (2012) documented a length change of 693 m during almost the same period (1992–2007). Areal estimates by Ghosh and Pandey (2013) and Pandey and others (2011) also differ from ours as they spectacle much higher deglaciation (almost double) during the study period (1992–2007). These variations can largely be explained by the inherent quality of data used (e.g. presence of temporal snow cover), obvious difficulties in precisely delineating the debris-covered snout and expertise of the analyst. However, despite differing in magnitude, the reported trend of deglaciation seems in line with the present study which found that the deglaciation rate has reduced post-2000 period (Table 4). Moreover, our results show a good match with Shukla and Qadir (2016). They found that, while retreat rate increased slightly, deglaciation rate of the Pensilungpa glacier reduced significantly during post-2000. These trends are also apparent in our results (Table 4).

In the regional context, the average retreat of the Pensilungpa glacier is lower than that of the other glaciers in the region. Kamp and others (2011) monitored 13 glaciers of the Greater Himalaya Range and reported an average retreat of ~20 m a^{-1} (average of ten glaciers) during 1990–2003, which increased to ~34 m a^{-1} during 2003–08 (Table 5). They also reported advancement of a few glaciers (e.g. Parkachik). Ali and others (2017) assessed 45 glaciers of the Lidder basin and reported an average retreat of 20.6 ± 7.3 m a^{-1} between 1996 and 2014. Shukla and Qadir (2016) also assessed five glaciers of Suru/Doda basin and noted an average length decrease of 7.8 m a^{-1}. Patel and others (2018) studied 29 glaciers of Miyar basin and found that these glaciers have retreated at a rate of 9.6 ± 5.2 m a^{-1} between 1989 and 2014. A recent study by Kaushik and others (2019) noted an average retreat of 12.44 ± 3.1 m a^{-1} during 1979–2017 for the 48 glaciers of Bhaga basin (Table 5). The area loss rate of the Pensilungpa glacier is comparable to the glaciers of the Ravi basin (Chand and Sharma, 2015) and the Chandra-Bhaga basin (Pandey and Venkataraman, 2013), but consistently lower than all other monitored basins of the western Himalaya (Table 5).

The SLA monitoring in this study shows a total upshift of 137 m during 1993–2016. However, a notable fluctuation in decadal scale has been observed (Section 4.1). Earlier, Shukla and Qadir (2016) found an average SLA increase of 207 m for the selected five glaciers of Suru/Doda basin and 280 m particularly for Pensilungpa glacier between 1977 and 2011. Thus, our observed SLA trends are in line with these reported measurements. Similar upshifting trends have also been observed in the other basins of western Himalaya (Negi and others, 2013; Pandey and others, 2013; Garg and others, 2017).

The Pensilungpa glacier has also been considered earlier for SIV estimation. Bhushan and others (2018) noticed that the lower portion of this glacier (up to ~2 km distance from snout) is nearly stagnant with SIV < 10 m a^{-1} while upstream portion of main trunk is active (SIV > 10 m a^{-1}). Our results also confirm similar spatial variations wherein the lower parts were found consistently stagnant during all the studied periods whereas upper portion remained active throughout (Fig. 6). Comparison of the temporal velocity variations is restricted by unavailability of such previous measurements on the glacier. However, trends of SIV reduction as observed in this study are comparable to that of previous studies conducted in the nearby basins of the western Himalaya which also report continuous glacier slowdown (Azam and others, 2012; Garg and others, 2017; Singh and others, 2018).

Earlier estimates of SEC demonstrate that the Pensilungpa glacier has been losing mass since 1960s (Pandey and others, 2011; Vijay and Braun, 2018; Bhushan and others, 2018). Pandey and others (2011) found a downwasting ranging from −0.73 to −2.19 m a^{-1} in the LAZ of this glacier between 1962 and 2003. Recently, Vijay and Braun (2018) quantified a downwasting of

https://doi.org/10.1017/jog.2021.84 Published online by Cambridge University Press

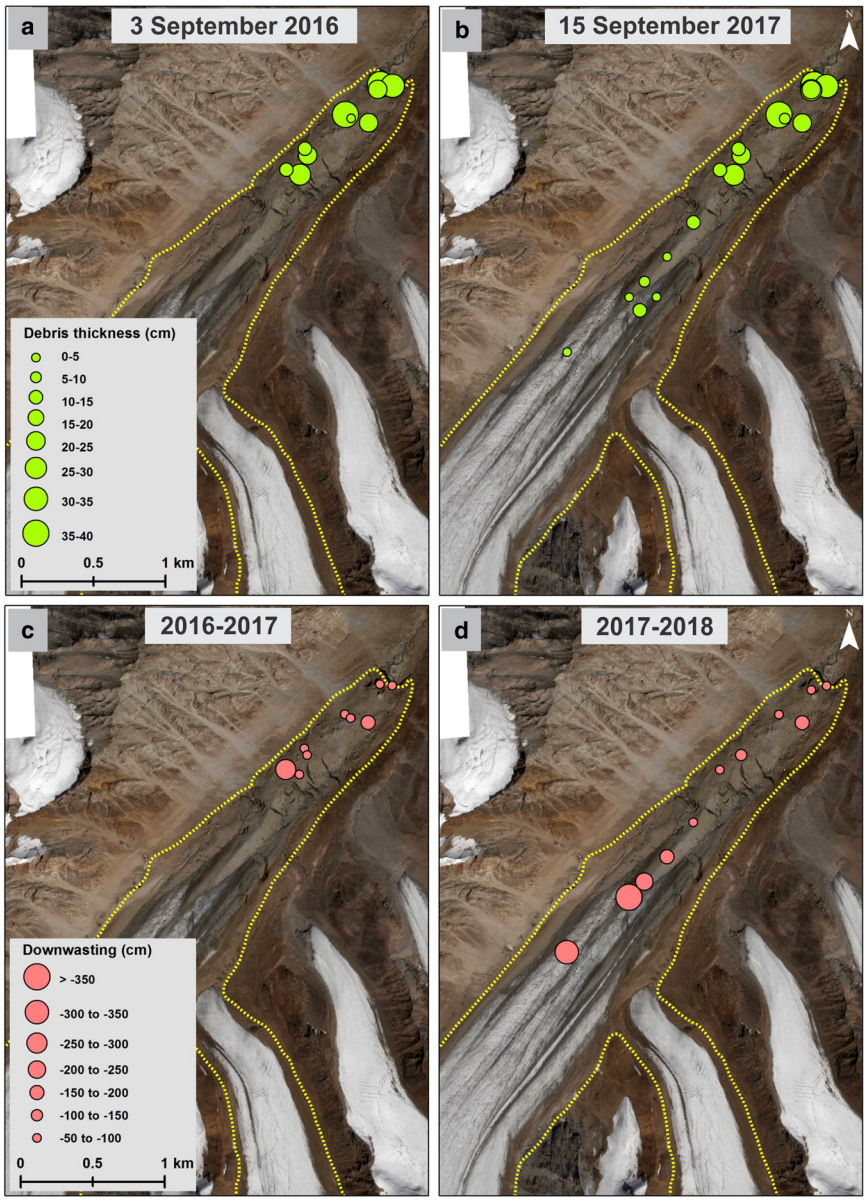

Fig. 7. Debris thickness on Pensilungpa glacier observed in the field during (a) 2016 and (b) 2017. The debris thickness near snout region reaches >40 cm and gradually decreases with increasing distance from snout. Figure also displays the field measured downwasting during 2016–2017 and 2017–2018. Note a clear influence of debris thickness on melting as higher downwasting is evident in upper ablation regions where debris thickness is lower (<5 cm) while less downwasting is apparent in lower ablation regions where debris is thick (~40 cm).

-0.63 ± 0.10 m a^{-1} during 2000–2012 for Pensilungpa glacier. In view of this, our SEC results (-0.88 ± 0.04 m a^{-1}) observed between 2000 and 2017 seem to be in line with these measurements. Moreover, regional SEC estimates of -0.66 ± 0.09 m a^{-1} (2000–2008) by Kääb and others (2012) for the entire Jammu and Kashmir, and -0.50 ± 0.28 m a^{-1} (2000–2012) for the Zanskar region also confirm significant and continuous mass wastage in the study area.

Comparing the spatial map of SEC of Pensilungpa glacier to that of previous studies (Fig. 8), it is evident that our estimates are in accordance with the Pandey and others (2011), who reported maximum downwasting in the upper ablation area of the glacier and also a slight elevation increase in the lower ablation portion at some places (Fig. 8). Field observation also confirms the presence of several ice mounds on glacier possibly developed due to surface uplift (Fig. 2). Further interpretation of SEC patterns in Figure 8 is provided in Section 5.3.

Moreover, we have observed higher lowering near the junction of right bank tributary glaciers to the main trunk which is also evident in the spatial SEC map of Pandey and others (2013) (Fig. 8). Our spatial SEC map deviates from Vijay and Braun (2018) which shows slightly higher downwasting (in order of -1 to -2 m a^{-1}) in the middle ablation portion. This deviation may be due to redistribution of ice mounds in this portion as observed during the field visits, which indeed gives the impression of elevation increase. Nevertheless, averaged downwasting over the entire glacier estimated by Vijay and Braun (2018) study is comparable to our estimations.

5.2. Glacier stagnation: evidence

Results of almost all the monitored parameters including length, area, debris cover, SLA, SIV and SEC indicate toward a depleting pattern of the Pensilungpa glacier during 1993–2016 (Sections 4.1 and 4.2). Climate trends reveal a clear rise in the mean annual temperature (0.77°C) and considerably high increase in the mean annual minimum temperature (1.3°C) over the last century. The temperature rising trend further accelerated over the last two to three decades (Shukla and others, 2020). A recent study by Mehta and others (2021) linked depleting pattern of the Pensilungpa glacier to this temperature rise. However, assessment on decadal scale reveals that the glacier wastage was higher during 1993–2000 which subsequently reduced in the time frame 2000–16. The relative area loss rate was lower ($0.09 \pm 0.09\%$ a^{-1}) during 2000–16 as compared to 1993–2000 ($0.17 \pm 0.24\%$ a^{-1}). Slowdown rates were also higher during 1993/94–1999/00

https://doi.org/10.1017/jog.2021.84 Published online by Cambridge University Press

Table 4. Comparison of length and area changes of this study with that of previous studies of corresponding study period for Pensilungpa glacier

Length change over different time periods			Area change over different time periods			References
Average retreat rate (m a^{-1})	Pre-2000 retreat rate (m a^{-1})	Post-2000 retreat rate (m a^{-1})	Average area loss (km^2 a^{-1})	Pre-2000 area loss (km^2 a^{-1})	Post-2000 area loss (km^2 a^{-1})	
1993–2016; 6.62 ± 2.11	1993–2000; 5.16 ± 6.92	2000–2016; 7.25 ± 3.03	1993–2016; 0.02 ± 0.01	1993–2000; 0.02 ± 0.04	2000–2016; 0.01 ± 0.02	This study
1977–2009/13; 7.64 ± 2.69	1992–2000; 7.70 ± 8.00	2000–2009/19; 7.78 ± 6.21	1992–2009; 0.14	1992–2000; 0.28	2000–2009; 0.02	Shukla and Qadir (2016)
1992–2001; 46.20	1992–2001; 77.00	2001–2007; 0.00	1992–2007;0.20	1992–2001; 0.44	2001–2007; 0.16[a]	Ghosh and Pandey (2013); Shukla and Qadir (2016)
1992–2006; 67.57	1992–2002; 88.90	2002–2006; 14.25	1992–2007; 0.29	1992–2001; 0.44	2001–2007; 0.29	Kamp and others (2011); Pandey and others (2011)

[a]Increase in glacier area.

(4.73% a^{-1}) as compared to 1999/00–2016/17 (1.14% a^{-1}). Here, results of SLA reveal a sharp ascend of snowline (180 m) during 1993–2000 indicating a low accumulation during this period which possibly led to higher deglaciation and drastic dropdown in the SIV. However, during 2000–2017, the SLA descended only by 43 m which is in compliance with observed reduction in slowdown and deglaciation rates. In synchronization with deglaciation and SIV, the debris-growth rate was also significantly higher during 1993–2000 (6.67 ± 0.41% a^{-1}) followed by a steep cut (0.09 ± 0.09% a^{-1}) during 2000–2016. During recession, as the glacier ice melts, debris mantle over it is left behind leading to an increase in the spatial extent of debris (Thompson and others, 2016; Ali and others, 2017). Here the only exception is snout retreat parameter which, in contrast to prevailing trend of generalized slowdown of glacier depletion rate, increased slightly in the recent decade (2000–16: 7.25 ± 3.03 m a^{-1}) as compared to the previous one (1993–2000: 5.16 ± 6.92 m a^{-1}). This increase in the retreat rate appeared to be induced by terminus environment and may not be directly linked to climate. This is explainable as an active dry-calving (break-off of ice blocks) and collapse of the ice-cave ceilings (due to undercutting by the subglacial waters and related seepage) have been observed in snout portion during all the field visits (Fig. 9). Large ice blocks are continuously being detached from the glacier in this part (Fig. 9). Hence, it appears that these dry calving and ice-cave collapse have probably led to slightly higher retreat in the recent decade. Further, it may be noted that the current and dominant process of ablation in the glacier is downwasting. In this study, downwasting has only been calculated for the 2000–17 period. However, comparing with Pandey and others (2011) who have calculated extensive downwasting on this glacier (−0.76 to −2.19 m a^{-1}) during 1992–2003, it can be asserted that the SEC rates have also reduced after 2000. These multiparametric observations confirm that the glacier is heading toward stagnation. Also, the spatial distribution of SIV elucidates that the lower portion of the glacier (up to ∼1.5 km distance from the snout) has become almost stagnant.

5.3. Glacier stagnation: causes

Glacier stagnation results from a chain of processes: firstly, an inadequate snow supply/mass input into the glacier (evident from ascending SLA) leads to glacier slowdown, downwasting and deglaciation (dimensional reduction) (see Sections 4.1 and 4.2). Downwasting and deglaciation result in an accumulation of debris on the glacier surface (Ali and others, 2017; Garg and others, 2017; Section 4.1). Here, the SIV plays a major role in redistribution, mobilization and removal of debris cover from the glacier system (Schroder and others, 2000; Quincey and others, 2009). Reduced glacier velocities negatively impact the efficient debris transfer mechanism of the glacier and hence the debris cover gradually thickens and expands up-glacier. Thus, the continuous increase of debris cover during 1993–2016 (2.86 ± 0.29% a^{-1}) and greater debris thickness near the snout region (>40 cm) indicate that these processes are active on the glacier.

The debris thickness distribution, though heterogeneous, largely follows a common pattern such that the debris thickness (a) increases from central flowline toward margins and (b) decreases with increasing distance from snout (Anderson and Anderson, 2018). Our field observations also confirm a very thick debris cover (∼40 cm) near the snout regions and thin debris-covered patches (2–5 cm) on up-glacier side. The debris thickness plays a major role in regulating the melt rates. Field measurements show comparatively low downwasting near the snout region of the Pensilungpa glacier where the debris is

https://doi.org/10.1017/jog.2021.84 Published online by Cambridge University Press

Table 5. Comparison of retreat and area loss rates of Pensilungpa glacier with those in surrounding basins

Glacier/basin/ region	Number of glaciers	Average area (km^2)	Average length (km)	Study period	Average retreat and deglaciation	References
Pensilungpa	1	14.67 ± 0.29	8.51	1993–2016	6.62 ± 2.11*	This study
Zanskar	10	NA	NA	1990–2003	20*	Kamp and others (2011)
Zanskar	5	NA	NA	2003–2008	27*	Kamp and others (2011)
Zanskar	5	NA	NA	1977–2013	7.8*	Shukla and Qadir (2016)
Chandra-Bhaga	15	25.18	10.25	1980–2010	15.5*	Pandey and Venkataraman (2013)
Lidder	45	2.12	NA	1996–2014	20.6*	Ali and others (2017)
Miyar	29	7.83	NA	1989–2014	9.6*	Patel and others (2018)
Bhaga	48	4.96	NA	1979–2017	12.44*	Kaushik and others (2019)
Pensilungpa	1	14.67 ± 0.29	8.51	1993–2016	0.11 ± 0.03†	This study
Zanskar	5	NA	NA	1977–2013	0.41†	Shukla and Qadir (2016)
Warwan	230	3.24	NA	1962–2002	0.48†	Brahmbhatt and others (2012)
Bhut	140	3.05	NA	1962–2002	0.23†	Brahmbhatt and others (2012)
Lidder	45	2.12	NA	1996–2014	0.67†	Ali and others (2017)
Ravi	157	0.80	NA	1971–2013	0.11†	Chand and Sharma (2015)
Chandra	116	6.00	NA	1962–2001/04	0.48†	Kulkarni and others (2011)
Bhaga	231	1.67	NA	2001–2011	0.16†	Birajdar and others (2014)
Chandra-Bhaga	15	25.18	10.25	1980–2010	0.08†	Pandey and Venkataraman (2013)
Beas	224	1.87	NA	1972–2006	0.34†	Dutta and others (2012)

NA, not available in the source study; *, retreat (m a^{-1}); †, deglaciation (% a^{-1}).

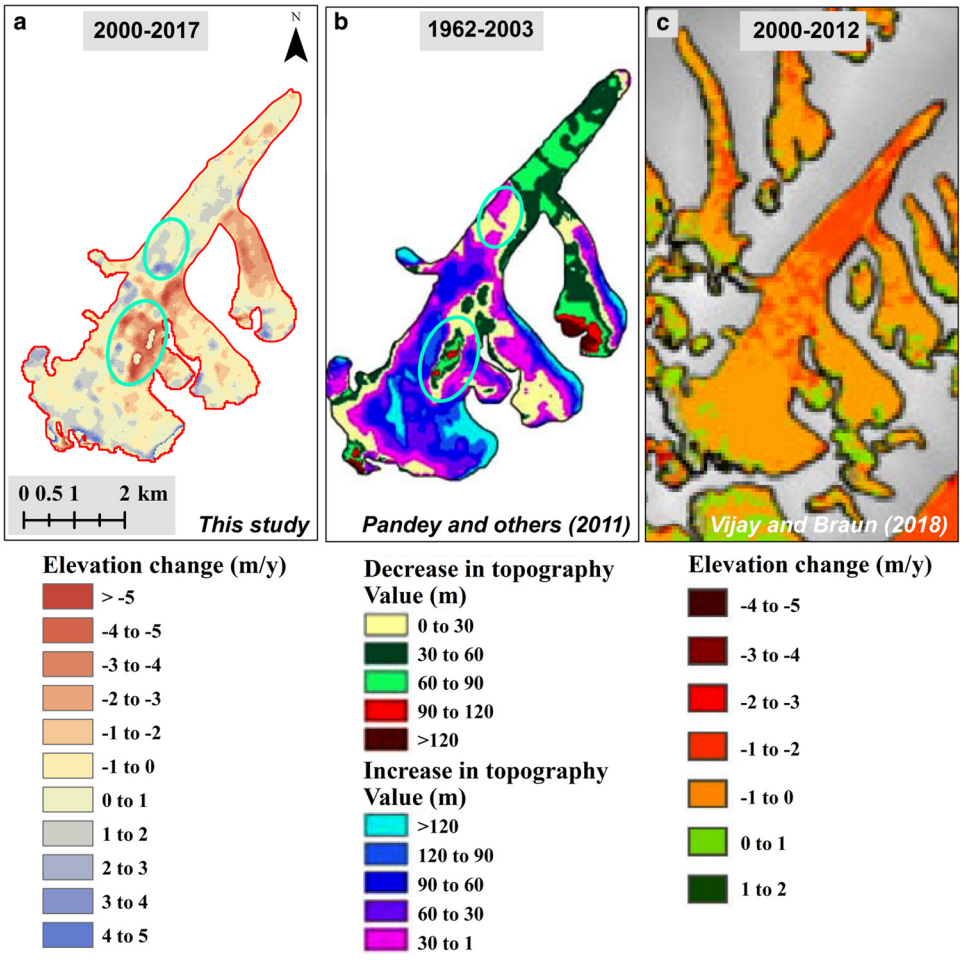

Fig. 8. Comparison of surface elevation changes estimation of this study with the previous studies. Circled areas on panel (a) and panel (b) show a similar trend of elevation change. Large difference in elevation change pattern at lower ablation zone may be due to large difference in the study periods and presence of debris cover (thickness >10 cm) which grew (by ~66%) during the study period (1993–2016) and exerting insulating effect. Permissions were obtained from Springer and Elsevier to reprint the figures from Pandey and others (2011) and Vijay and Braun (2018), respectively.

thick while higher downwasting has been observed over bare ice (covered with debris dust) and on the regions where debris thickness is generally less (Fig. 7). Here, we have also quantified the correlation between debris thickness and downwasting. A good correlation coefficient ($r^2 = 0.51$) between debris thickness measured in 2016 and downwasting during 2016–2017 was found (Fig. 10a). Similarly, an improved correlation ($r^2 = 0.56$) between debris thickness and downwasting during 2017–2018 has been

https://doi.org/10.1017/jog.2021.84 Published online by Cambridge University Press

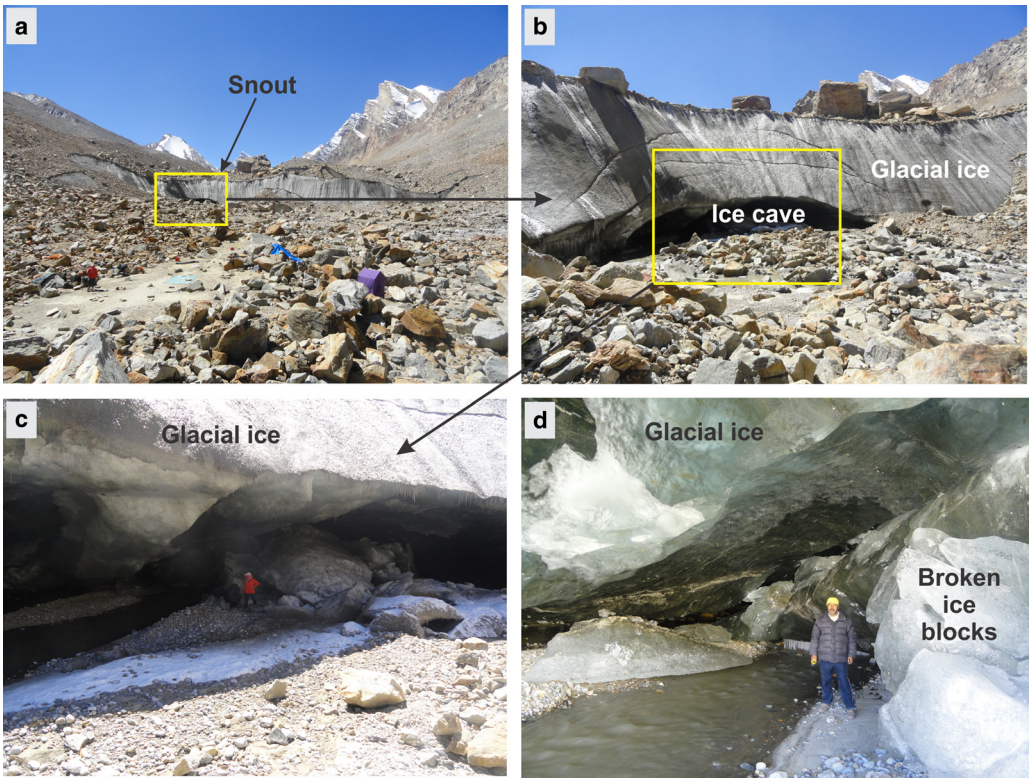

Fig. 9. Snout characteristics of the Pensilungpa glacier. A large cave can be seen at the snout of this glacier where frequent activities of dry calving (i.e. direct breaking-off of ice blocks) have been observed during the field visits. Field photographs are of the year 2017.

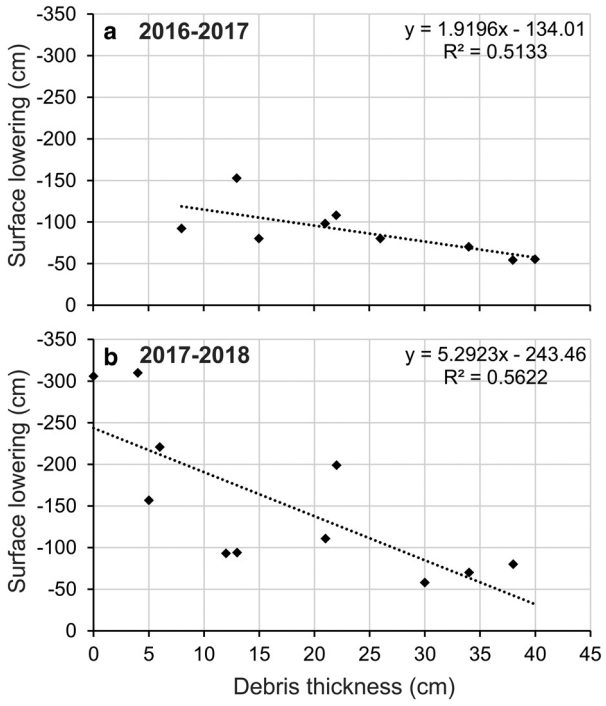

Fig. 10. Correlation between debris thickness and downwasting observed on the field during (a) 2016–17 and (b) 2017–18. The correlation is apparently negative which implies that higher the debris thickness lower the downwasting.

observed (Fig. 10b). These findings further confirm a significant influence of the debris thickness on melt rates.

Given the influence of the debris thickness on melting, the observed debris thickness distribution has the following implications. Firstly, the thick debris cover probably protected the glacier margins which is the most likely reason of observed reduction in deglaciation rates of the Pensilungpa glacier in the recent decade. Eventually, thick debris cover, stable/insulated glacier margins and the impedance created by the side valley-walls collectively contributed in dragging the glacier velocity down, which lead to stagnation of lower portion of the glacier. Secondly, the observed distribution of the debris thickness has promoted a characteristic inverted ablation gradients (Figs 6b, 7) on the glacier which have long been recognized as one of the prime factors underpinning the distinct/unique response of the debris-covered glaciers (Scherler and others, 2011; Benn and others, 2012; Sharma and others, 2016). This inverted ablation coupled with the decrease in glacier thickness reduced the driving stress (Quincey and others, 2009; Benn and others, 2012), which causes further stagnation. Figure 8 also shows a shift in SEC trends at LAZ over the time. Though the different color gradients and the different units in panels (a) and (b) of Figure 8 make direct comparison difficult, it can be asserted that the magnitude of lowering at LAZ was slightly higher during 1962–2003 (Pandey and others, 2011). However, owing to notable insulating effect of debris, the lowering rates have reduced in the recent period (2000–2017). Moreover, owing to progressive reduction in velocity (as evident by the current trend of slowdown) and continued downwasting, the stagnant zone is likely to extend further up.

5.4. Stagnation: implications on glacio-geomorphic processes and resulting ice cliffs

Annual field measurements show a pronounced location melting on the glacier in the recent years, i.e. for 2016–17 and 2017–18 (Fig. 7). Geodetic measurements also confirm a notable average downwasting of -0.88 ± 0.04 m a^{-1} between 2000 and 2017. Interestingly, in spite of this observed overall downwasting, long-term SEC calculations (2000–17) reveal almost no net change in overall surface elevation in glacier parts 2–5 km up-glacier and even a slight surface uplift has been noticed (Fig. 6). Earlier,

https://doi.org/10.1017/jog.2021.84 Published online by Cambridge University Press

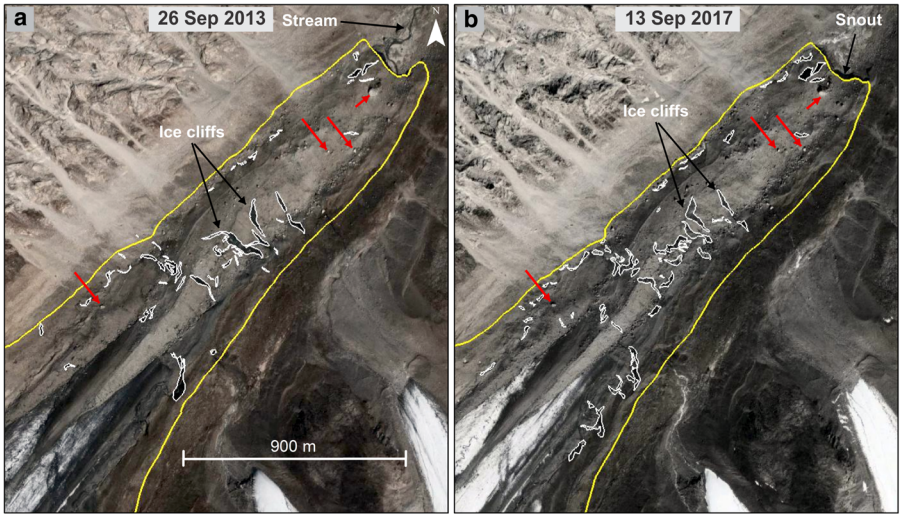

Fig. 11. Temporal evolution of lower ablation zone (~2 km upstream) between (a) 2013 and (b) 2017, observed using high-resolution images from GoogleEarth™ (Centre National d'Études Spatiales (CNES), France/Airbus) dated 26 September 2013 and 13 September 2017, respectively. The stagnant state of this portion is evident from the stationary position of the supraglacial markers (boulders; marked by red arrows) during 2013–2017. Progressive development of ice cliff is also apparent on the temporal images which suggests that an active back-wasting process is operative on the glacier.

Thomson and others (2016) also noticed striping of downwasting alternating with the areas of apparent uplift, with values up to ±50 m during 2010–12 and 2012–15 on the Ngozumpa glacier of Nepal. They stressed that the striped pattern is the resultant of displacement of surface topography down-glacier by ice flow. Here, evaluating our results in light of velocity results, it is evident that uplift has occurred on dynamically active part (i.e. ~2–5 km from snout) directly up-glacier of the lower stagnant zone. We interpret it as bulging-up of ice mass in this region, possibly induced by contrasting velocities of active upper portion and stagnant lower region which balances the melting of ice resulting in no net change in overall surface elevation.

The slow moving (<10 m a^{-1}) and gently sloping (<6–8°) glacier tongue, supported by prevailing negative mass-balance regimes, forms favorable conditions for the formation and development of the glacial lakes and ice cliffs (Sakai and others, 2002; Miles and others, 2016; Thompson and others, 2016). On the Pensilungpa glacier, a few supraglacial ponds have been observed (Fig. 4) which, though small in size, are likely to expand rapidly due to expected melting of dusty ice-walls surrounding the ponds (Benn and others, 2001; Sakai and others, 2002). Moreover, the Pensilungpa glacier is riddled with ice cliffs. Here, a detailed assessment of lower tongue (~2 km upstream) has been carried out using high-resolution images from GoogleEarth™ (Centre National d'Études Spatiales (CNES), France/Airbus) for 2013 and 2017 to assess the dynamics of these ice cliffs (Fig. 11). Visual inspection of this portion shows no sign of movement. Most of the surface features have been preserved during 2013–2017. For instance, well-identifiable big boulders present on the surface remained stationary between 2013 and 2017 confirming stagnant state of underlying ice. These observations corroborate well with the results obtained by correlating Landsat images (Fig. 6) in this study. However, the only notable activity in this portion is the backwasting of ice cliffs. Ice cliffs are the typical features of debris-covered glaciers (Sakai and others, 2002; Benn and others, 2012). The average melt rate at an ice cliff has been reported to be ~10 times that of debris-covered areas (Sakai and others, 1998, 2002). Earlier, several studies have highlighted significant contribution of ice cliffs on total mass wastage of a glacier which may range from ~8 to 40% even they occupy small fraction of total glacier area (Sakai and others, 1998, 2002; Immerzeel and others, 2014; Thomson and others, 2016). In the present study, we digitized all the ice cliffs present on the lower ~2 km portion interactively on high-resolution images from GoogleEarth™ for the years 2013 and 2017. Results show a total number of 52 ice cliffs with a total area of 33 854 m^2 in 2013. In 2017, the total number and area of ice cliffs increased significantly to 77 and 47 607 m^2, respectively. It is important to note that the dark shadows caused by steep ice cliffs make it challenging to demarcate their borders precisely even on the high-resolution images and may introduce sizable error. However, a clear increase of ~48% in number and 41% in area of ice cliffs within such a short period of time (i.e. ~4 years) clearly indicates that the backwasting of ice cliffs is the dominant mechanism of mass loss in this portion.

6. Conclusions

This study has attempted to assess the present conditions as well as the evolution of the Pensilungpa glacier during 1990–2017. For this, multiple glacier parameters namely length, area, debris cover, debris thickness, SLA, SIV, SEC and ice cliffs were evaluated using field and remote-sensing data acquired between 1993 and 2017. The results show that, though the depletion rate is comparatively lower as compared to the other western Himalayan glaciers, the glacier is in depleting phase with a clear reduction in almost all the monitored glacier parameters, with a notable increase in SLA and concomitant growth in debris cover area during 1993–2016. A clear temperature increase (especially in mean annual minimum temperature) in the study region over the last century and particularly over the last two to three decades seems to be the prime driver of observed glacier changes. However, overall glacier wastage rate has reduced in the recent time period (2000–17) as compared to the previous one. From the results, it has been inferred that a comparatively less SLA upshift during 2000–17 and remarkable debris area and thickness increase during 1993–2000 might be the probable reasons of this reduction in depletion rates. Further, the SIV results confirm that the LAZ (up to 2 km up-glacier) has remained stagnant during the study period. The debris thickness characteristics of the glacier can be largely ascribed to this stagnation.

The thickness of the supraglacial debris gradually decreases from the snout up-glacier and from the margins to the central flowline. Such debris thickness distribution has not only insulated the glacier margins but also contributed in observed slowdown. Further, debris thickness-induced differential melting (i.e. less downwasting near snout region and high downwasting up-glacier) has resulted in characteristic slope inversion, which also contributed in the stagnation by reducing the driving stress. Stagnation has had several implications: First, lower stagnant ablation portion has caused slight bulging in the upper dynamically active part of ABZ. Second, slow moving debris-covered zone has

https://doi.org/10.1017/jog.2021.84 Published online by Cambridge University Press

facilitated the development of supraglacial ponds which are low in number and small in extent but are likely to grow in future. Third, numerous ice cliffs developed on the lower ablation portion (up to ~2 km up-glacier). Systematic assessment of these ice cliffs between 2013 and 2017 reveals a marked increase in their number and area. Thus, given the insulated glacier margins and reducing glacier velocities, back-wasting of ice cliffs dominates the ablation process in the glacier.

Supplementary material. The supplementary material for this article can be found at https://doi.org/10.1017/jog.2021.84

Acknowledgement. The authors are thankful to the Director, Wadia Institute of Himalayan Geology for providing required facilities to carry out this work. A.S. thanks the Secretary, Ministry of Earth Sciences, Government of India for facilitating the study. The authors extend sincere gratitude to Dr Hester Jiskoot (Associate Chief Editor), Dr Neil Glasser (Scientific Editor) and the two anonymous referees whose detailed comments have significantly improved the paper. P.K.G. acknowledges the research grant from National Post-Doctoral Fellowship (NPDF) award (PDF/2020/000103) from the Department of Science and Technology, Government of India and the Indian Institute of Technology Indore, India for hosting NPDF tenure.

Author contributions. P.K.G. and A.S. designed the study and wrote the paper. P.K.G. performed calculations and generated the figures. S.G. and B.Y. estimated field-velocity. V.K., M.M., A.S. and S.G. contributed to field measurements. All the authors discussed the results and contributed to the final form of the article.

References

Ali I, Shukla A and Romshoo SA (2017) Assessing linkages between spatial facies changes and dimensional variations of glaciers in the upper Indus Basin, western Himalaya. *Geomorphology* **284**, 115–129. doi: 10.1016/j.geomorph.2017.01.005

Anderson LS and Anderson RS (2018) Debris thickness patterns on debris-covered glaciers. *Geomorphology* **311**, 1–12. doi: 10.1016/j.geomorph.2018.03.014

Archer DR and Fowler HJ (2004) Spatial and temporal variations in precipitation in the Upper Indus Basin, global teleconnections and hydrological implications. *Hydrology and Earth System Sciences* **8**, 47–61. doi: 10.5194/hess-8-47-2004

Armstrong RL (2010) The glaciers of the Hindu Kush-Himalayan region: a summary of the science regarding glacier melt/retreat in the Himalayan, Hindu Kush, Karakoram, Pamir, and Tien Shan mountain ranges. International Centre for Integrated Mountain Development (ICIMOD).

Azam MF and 10 others (2012) From balance to imbalance: a shift in the dynamic behaviour of Chhota Shigri glacier, western Himalaya, India. *Journal of Glaciology* **58**(208), 315–324. doi: 10.3189/2012JoG11J123

Benn DI and 9 others (2012) Response of debris-covered glaciers in the Mount Everest region to recent warming, and implications for outburst flood hazards. *Earth Science Reviews* **114**(1–2), 156–117. doi: 10.1016/j.earscirev.2012.03.008

Benn DI, Wiseman S and Hands KA (2001) Growth and drainage of supraglacial lakes on debris-mantled Ngozumpa Glacier, Khumbu Himal, Nepal. *Journal of Glaciology* **47**(159), 626–638. doi: 10.3189/172756501781831729

Berthier E, Cabot V, Vincent C and Six D (2016) Decadal region-wide and glacier-wide mass balances derived from multi-temporal ASTER satellite digital elevation models. Validation over the Mont-Blanc area. *Frontiers in Earth Science* **4**(63), 1–16. doi: 10.3389/feart.2016.00063

Bhambri R, Bolch T, Chaujar RK and Kulshreshta SC (2011) Glacier changes in the Garhwal Himalaya, India, 1968–2006 based on remote sensing. *Journal of Glaciology* **57**(203), 543–556. doi: 10.3189/002214311796905604

Bhattacharya A and 5 others (2016) Overall recession and mass budget of Gangotri Glacier, Garhwal Himalayas, from 1965 to 2015 using remote sensing data. *Journal of Glaciology* **62**(236), 1115–1133. doi: 10.1017/jog.2016.96

Bhushan S, Syed TH, Arendt AA, Kulkarni AV and Sinha D (2018) Assessing controls on mass budget and surface velocity variations of glaciers in Western Himalaya. *Scientific Reports* **8**(1), 1–11. doi: 10.1038/s41598-018-27014-y

Bhushan S, Syed TH, Kulkarni AV, Gantayat P and Agarwal V (2017) Quantifying changes in the Gangotri Glacier of Central Himalaya: evidence for increasing mass loss and decreasing velocity. *IEEE Journal of Selected Topics in Applied Earth Observations and Remote Sensing* **10**(12), 5295–5306. doi: 10.1109/JSTARS.2017.2771215

Bhutiyani MR, Kale VS and Pawar NJ (2010) Climate change and the precipitation variations in the northwestern Himalaya: 1866–2006. *International Journal of Climatology* **30**(4), 535–548. doi: 10.1002/joc.1920

Birajdar F, Venkataraman G, Bahuguna I and Samant H (2014) A revised Glacier Inventory of Bhaga Basin Himachal Pradesh, India: current status and recent Glacier variations. *ISPRS Annals of the Photogrammetry, Remote Sensing and Spatial Information Sciences* **II-8**(December), 37–43.

Bolch T, Pieczonka T and Benn DI (2011) Multi-decadal mass loss of glaciers in the Everest area (Nepal Himalaya) derived from stereo imagery. *The Cryosphere* **5**(2), 349–358. doi:10.5194/tc-5-349-2011.

Bolch T and 11 others (2012) The state and fate of Himalayan Glaciers. *Science (New York, N.Y.)* **336**(6079), 310–314. doi: 10.1126/science.1215828

Brahmbhatt RM, Bahuguna IM, Rathore BP, Kulkarni AV, Nainwal HC, Shah RD and Ajai (2012) A comparative study of deglaciation in two neighbouring basins (Warwan and Bhut) of Western Himalaya. *Current Science* **103**(3), 298–304.

Chand P and Sharma MC (2015) Glacier changes in the Ravi basin, northwestern Himalaya (India) during the last four decades (1971–2010/13). *Global and Planetary Change* **135**, 133–147. doi: 10.1016/j.gloplacha.2015.10.013

Dutta S, Ramanathan AL and Linda A (2012) Glacier fluctuation using satellite data in Beas basin, 1972–2006, Himachal Pradesh, India. *Journal of earth system science* **121**(5), 105–112. doi:10.1007/s12040-012-0219-1.

Gardelle J, Berthier E, Arnaud Y and Kääb A (2013) Region-wide glacier mass balances over the Pamir-Karakoram-Himalaya during 1999-2011. *The Cryosphere* **7**(6), 1263–1286. doi: 10.5194/tc-7-1263-2013

Garg PK, Shukla A and Jasrotia AS (2019) On the strongly imbalanced state of glaciers in the Sikkim, eastern Himalaya, India. *Science of the Total Environment* **691**, 16–35. doi: 10.1016/j.scitotenv.2019.07.086

Garg PK, Shukla A, Tiwari RK and Jasrotia AS (2017) Assessing the status of glaciers in part of the Chandra basin, Himachal Himalaya: a multiparametric approach. *Geomorphology* **284**, 99–114. doi: 10.1016/j.geomorph.2016.10.022

Ghosh S and Pandey AC (2013) Estimating the variation in glacier area over the last 4 decade and recent mass balance fluctuations over the Pensilungpa glacier, J&K, India. *Global Perspectives on Geography* **1**(4), 58–65.

GLIMS (2015) *GLIMS Glacier Database Version 1*. Boulder, CO: National Snow and Ice Data Center. doi: 10.7265/N5V98602

Hall DK, Bayr KJ, Schöner W, Bindschadler RA and Chien JY (2003) Consideration of the errors inherent in mapping historical glacier positions in Austria from the ground and space (1893–2001). *Remote Sensing of Environment* **86**(4), 566–577. doi: 10.1016/S0034-4257(03)00134-2

Harris IP, Jones PD, Osborn TJ and Lister DH (2014) Updated high-resolution grids of monthly climatic observations – the CRU TS3. 10 Dataset. *International Journal of Climatology* **34**(3), 623–642. doi: 10.1002/joc.3711

Heid T and Kääb A (2012) Evaluation of existing image matching methods for deriving glacier surface displacements globally from optical satellite imagery. *Remote Sensing of Environment* **118**, 339–355. doi: 10.1016/j.rse.2011.11.024

Hoelzle M, Haeberli W, Dischl M and Peschke W (2003) Secular glacier mass balances derived from cumulative glacier length changes. *Global and Planetary Change* **36**(4), 295–306. doi: 10.1016/S0921-8181(02)00223-0

Immerzeel WW and 6 others (2014) High-resolution monitoring of Himalayan glacier dynamics using unmanned aerial vehicles. *Remote Sensing of Environment* **150**, 93–103. doi: 10.1016/j.rse.2014.04.025

Kääb A, Berthier E, Nuth C, Gardelle J and Arnaud Y (2012) Contrasting patterns of early twenty-first-century glacier mass change in the Himalayas. *Nature* **488**(7412), 495–498. doi: 10.1038/nature11324

Kamp U, Byrne M and Bolch T (2011) Glacier fluctuations between 1975 and 2008 in the Greater Himalaya Range of Zanskar, southern Ladakh. *Journal of Mountain Science* **8**(3), 374–389. doi: 10.1007/s11629-011-2007-9

Kargel JS, Cogley JG, Leonard GJ, Haritashya U and Byers A (2011) Himalayan glaciers: the big picture is a montage. *Proceedings of the*

National Academy of Sciences **108**(36), 14709–14710. doi: 10.1073/pnas.1111663108

Kaushik S, Dharpure JK, Joshi PK, Ramanathan AL and Singh T (2019) Climate change drives glacier retreat in Bhaga basin located in Himachal Pradesh, India. *Geocarto International* **35**(11), 1179–1198. doi: 10.1080/10106049.2018.1557260

Kulkarni AV, Rathore BP, Singh SK and Bahuguna IM (2011) Understanding changes in the Himalayan cryosphere using remote sensing techniques. *International journal of remote sensing* **32**(3), 601–615. doi:10.1080/01431161.2010.517802.

Kumar GV, Kulkarni AV, Gupta AK and Sharma P (2017) Mass balance estimation using geodetic method for glaciers in Baspa basin, Western Himalaya. *Current Science* **113**(3), 486–492.

Leclercq PW and Oerlemans J (2012) Global and hemispheric temperature reconstruction from glacier length fluctuations. *Climate Dynamics* **38** (5–6), 1065–1079. doi: 10.1007/s00382-011-1145-7

Leprince S, Barbot S, Ayoub F and Avouac JP (2007) Automatic and precise orthorectification, coregistration, and subpixel correlation of satellite images, application to ground deformation measurements. *IEEE Transactions on Geoscience and Remote Sensing* **45**(6), 1529–1558. doi: 10.1109/TGRS.2006.888937

Mehta M, Kumar V, Garg S and Shukla A (2021) Little Ice Age glacier extent and temporal changes in annual mass balance (2016–2019) of Pensilungpa Glacier, Zanskar Himalaya. *Regional Environmental Change* **21**(2), 21–38. doi: 10.1007/s10113-021-01766-2.

Miles ES, Willis IC, Arnold NS, Steiner J and Pellicciotti F (2017) Spatial, seasonal and interannual variability of supraglacial ponds in the Langtang Valley of Nepal, 1999–2013. *Journal of Glaciology* **63**(237), 88–105. doi: 10.1017/jog.2016.120

Negi HS, Saravana G, Rout R and Snehmani (2013) Monitoring of great Himalayan glaciers in Patsio region, India using remote sensing and climatic observations. *Current Science* **105**(10), 1383–1392.

Nuth C and Kääb A (2011) Co-registration and bias corrections of satellite elevation data sets for quantifying glacier thickness change. *The Cryosphere* **5**(1), 271–290. doi: 10.5194/tc-5-271-2011

Pandey AC, Ghosh S, Nathawat MS and Tiwari RK (2011) Area change and thickness variation over Pensilungpa Glacier (J&K) using remote sensing. *Journal of the Indian Society of Remote Sensing* **40**(2), 245–255. doi: 10.1007/s12524-011-0134-y

Pandey P, Kulkarni AV and Venkataraman G (2013) Remote sensing study of snowline altitude at the end of melting season, Chandra-Bhaga basin, Himachal Pradesh, 1980–2007. *Geocarto International* **28**(4), 311–322. doi: 10.1080/10106049.2012.705336

Pandey AC, Nathawat MS and Ghosh S (2012) Morphometric control on glacier area changes in the Great Himalayan Range, Jammu and Kashmir, India. *Current Science* **102**(8), 1188–1193.

Pandey P and Venkataraman G (2013) Changes in the glaciers of Chandra–Bhaga basin, Himachal Himalaya, India, between 1980 and 2010 measured using remote sensing. *International Journal of Remote Sensing* **34**(15), 5584–5597. doi: 10.1080/01431161.2013.793464

Patel LK, Sharma P, Fathima TN and Thamban M (2018) Geospatial observations of topographical control over the glacier retreat, Miyar basin, Western Himalaya, India. *Environmental Earth Sciences* **77**(190), 1–12. doi: 10.1007/s12665-018-7379-5

Paul F and 10 others (2013) On the accuracy of glacier outlines derived from remote-sensing data. *Annals of Glaciology* **54**(63), 171–182. doi: 10.3189/2013AoG63A296

Quincey DJ, Luckman A and Benn D (2009) Quantification of Everest region glacier velocities between 1992 and 2002, using satellite radar interferometry and feature tracking. *Journal of Glaciology* **55**(192), 596–606. doi: 10.3189/002214309789470987

Rabatel A, Letréguilly A, Dedieu JP and Eckert N (2013) Changes in glacier equilibrium-line altitude in the western Alps from 1984 to 2010: evaluation by remote sensing and modeling of the morpho-topographic and climate controls. *The Cryosphere* **7**(5), 1455–1471. doi: 10.5194/tc-7-1455-2013

Racoviteanu AE, Paul F, Raup B, Khalsa SJ and Armstrong R (2009) Challenges and recommendations in mapping of glacier parameters from space: results of the 2008 Global Land Ice Measurements from Space (GLIMS) workshop, Boulder, Colorado, USA. *Annals of Glaciology* **50** (53), 53–69. doi: 10.3189/172756410790595804

Rodriguez E, Morris CS and Belz JE (2006) A global assessment of the SRTM performance. *Photogrammetric Engineering & Remote Sensing* **72**(3), 249–260. doi: 10.14358/PERS.72.3.249

Sakai A, Nakawo M and Fujita K (1998) Melt rate of ice cliffs on the Lirung Glacier, Nepal Himalayas, 1996. *Bulletin of Glacier Research* **16**, 57–66.

Sakai A, Nakawo M and Fujita K (2002) Distribution characteristics and energy balance of ice cliffs on debris-covered glaciers, Nepal Himalaya. *Arctic, Antarctic, and Alpine Research* **34**(1), 12–19. doi: 10.1080/15230430.2002.12003463

Scherler D, Bookhagen B and Strecker MR (2011) Spatially variable response of Himalayan glaciers to climate change affected by debris cover. *Nature Geoscience* **4**(3), 156–159. doi: 10.1038/ngeo1068

Scherler D and Strecker MR (2012) Large surface velocity fluctuations of Biafo Glacier, central Karakoram, at high spatial and temporal resolution from optical satellite images. *Journal of Glaciology* **58**(209), 569–580. doi: 10.3189/2012JoG11J096

Sharma P and 5 others (2016) Role of debris cover to control specific ablation of adjoining Batal and Sutri Dhaka glaciers in Chandra Basin (Himachal Pradesh) during peak ablation season. *Journal of Earth System Science* **125**(3), 459–473.

Shroder JF, Bishop MP, Copland L and Sloan VF (2000) Debris-covered glaciers and rock glaciers in the Nanga Parbat Himalaya, Pakistan. *GeografiskaAnnaler: Series A, Physical Geography* **82**(1), 17–31.

Shukla A and Garg PK (2019) Evolution of a debris-covered glacier in the western Himalaya during the last four decades (1971–2016): a multiparametric assessment using remote sensing and field observations. *Geomorphology* **341**, 1–4. doi: 10.1016/j.geomorph.2019.05.009.

Shukla A, Garg S, Mehta M, Kumar V and Shukla UK (2020) Temporal inventory of glaciers in the Suru sub-basin, western Himalaya: impacts of regional climate variability. *Earth System Science Data* **12**(2), 1245–1265. doi: 10.5194/essd-12-1245-2020

Shukla A and Qadir J (2016) Differential response of glaciers with varying debris cover extent: evidence from changing glacier parameters. *International Journal of Remote Sensing* **37**(11), 2453–2479. doi: 10.1080/01431161.2016.1176272

Singh KK and 5 others (2018) Temporal change and flow velocity estimation of Patseo glacier, Western Himalaya, India. *Current Science* **114**(4), 776–784. doi: 10.18520/cs/v114/i04/776-784

Steiner JF, Buri P, Miles ES, Ragettli S and Pellicciotti F (2019) Supraglacial ice cliffs and ponds on debris-covered glaciers: spatio-temporal distribution and characteristics. *Journal of Glaciology* **65**(252), 617–632. doi: 10.1017/jog.2019.40

Storey JC and Choate MJ (2004) Landsat-5 bumper-mode geometric correction. *IEEE Transactions on Geoscience and Remote Sensing* **42**, 2695–2703. doi: 10.1109/TGRS.2004.836390

Thompson S, Benn DI, Mertes J and Luckman A (2016) Stagnation and mass loss on a Himalayan debris-covered glacier: processes, patterns and rates. *Journal of Glaciology* **62**(233), 467–485. doi: 10.1017/jog.2016.37

Tiwari RK, Gupta RP and Arora MK (2014) Estimation of surface ice velocity of Chhota-Shigri glacier using sub-pixel ASTER image correlation. *Current Science* **106**(6), 853–859.

Vijay S and Braun M (2016) Elevation change rates of glaciers in the Lahaul-Spiti (Western Himalaya, India) during 2000–2012 and 2012–2013. *Remote Sensing* **8**(12), 1–16. doi: 10.3390/rs8121038

Vijay S and Braun M (2018) Early 21st century spatially detailed elevation changes of Jammu and Kashmir glaciers (Karakoram–Himalaya). *Global and Planetary Change* **165**, 137–146. doi: 10.1016/j.gloplacha.2018.03.014

Vincent C and 9 others (2013) Balanced conditions or slight mass gain of glaciers in the Lahaul and Spiti region (northern India, Himalaya) during the nineties preceded recent mass loss. *The Cryosphere* **7**(2), 569–582. doi: 10.5194/tc-7-569-2013

Zemp M and 10 others (2015) Historically unprecedented global glacier decline in the early 21st century. *Journal of Glaciology* **61**(228), 745–762. doi: 10.3189/2015JoG15J017

Zhou Y, Li Z, Li J, Zhao R and Ding X (2018) Glacier mass balance in the Qinghai–Tibet Plateau and its surroundings from the mid-1970s to 2000 based on Hexagon KH-9 and SRTM DEMs. *Remote sensing of Environment* **210**, 96–112. doi: 10.1016/j.rse.2018.03.020

https://doi.org/10.1017/jog.2021.84 Published online by Cambridge University Press